

See discussions, stats, and author profiles for this publication at: <https://www.researchgate.net/publication/231645597>

# Synthesis and Catalytic Properties for Phenylacetylene Hydrogenation of Silicide Modified Nickel Catalysts

ARTICLE *in* THE JOURNAL OF PHYSICAL CHEMISTRY C · SEPTEMBER 2010

Impact Factor: 4.77 · DOI: 10.1021/jp1050832

---

CITATIONS

24

READS

39

## 6 AUTHORS, INCLUDING:



Xiao Chen

Dalian University of Technology

30 PUBLICATIONS 181 CITATIONS

[SEE PROFILE](#)



Christopher T Williams

University of South Carolina

134 PUBLICATIONS 2,143 CITATIONS

[SEE PROFILE](#)



Changhai Liang

Dalian University of Technology

137 PUBLICATIONS 3,813 CITATIONS

[SEE PROFILE](#)

# Synthesis and Catalytic Properties for Phenylacetylene Hydrogenation of Silicide Modified Nickel Catalysts

Xiao Chen,<sup>†</sup> Anqi Zhao,<sup>†</sup> Zhengfeng Shao,<sup>†</sup> Chuang Li,<sup>†</sup> Christopher T. Williams,<sup>‡</sup> and Changhai Liang<sup>\*,†</sup>

Laboratory of Advanced Materials and Catalytic Engineering, School of Chemical Engineering, Dalian University of Technology, Dalian 116012, China, and Department of Chemical Engineering, Swearingen Engineering Center, University of South Carolina, Columbia, South Carolina 29208

Received: June 2, 2010; Revised Manuscript Received: August 21, 2010

Interstitial silicide-modified nickel, with high selectivity in some hydrogenation reactions, had been produced by dissolving silicon atoms into the nickel lattices. The metallic nickel was obtained by reducing the as-prepared high surface area NiO, followed by modification of the bulk nickel through silification of silane/H<sub>2</sub> at relatively low temperature and atmospheric pressure. The as-prepared materials were characterized by X-ray diffraction, magnetic measurements, X-ray photoelectron spectroscopy, transmission electron microscopy, energy dispersive X-ray spectroscopy, and temperature-programmed reduction. The results show nickel silicide formation involves the following sequence as a function of increasing temperature: Ni (cubic) → Ni<sub>2</sub>Si (orthorhombic) → NiSi (orthorhombic) → NiSi<sub>2</sub> (cubic). The insertion of Si atoms into the interstitial sites between Ni atoms resulted in a significant change in the unit cell lattice of nickel. All of the silicide-modified nickel materials were ferromagnetic at room temperature, and saturation magnetization values drastically decreased when Si is present. Silicide-modified nickel develops a thin silicon oxide layer during exposure to air, which can be removed by H<sub>2</sub>-temperature programmed reduction. The as-prepared bulk silicide-modified nickel showed above 92% styrene selectivity in the hydrogenation of phenylacetylene under 0.41 MPa H<sub>2</sub> and at 50 °C for 5 h. In addition, only low conversions were obtained for styrene hydrogenation under the same hydrogen pressure and temperature for 50 min. These results indicate that these novel silicide-modified nickels are promising catalysts for the selective hydrogenation of unsaturated hydrocarbons.

## 1. Introduction

Due to the strong interaction between their component elements, interstitial silicides of early transition metals have specific crystal and electronic structures different from that of their component metals. Such metal silicide materials are attracting increased attention in many fields, including complementary metal-oxide-semiconductor (CMOS) devices,<sup>1</sup> thin film coatings,<sup>2</sup> photoelectrocatalysts<sup>3</sup> and thermoelectric materials,<sup>4</sup> due to their unique physical and chemical properties.

Metal silicides formed from the dissolution of silicon atoms into metal lattices also have unusual structural and catalytic properties, especially in some selective hydrogenation reactions.<sup>5</sup> Nuzzo et al. first reported the synthesis of metal silicides by exposing supported metals to volatile silane. The material demonstrated high catalytic activity and selectivity for the competitive dehydrogenation and hydrogenolysis of cyclohexane.<sup>6</sup> Recently, Baiker et al.<sup>7</sup> indicated that amorphous Pd<sub>81</sub>Si<sub>19</sub> catalyst prepared by melt spinning demonstrated high selectivity to styrene using supercritical CO<sub>2</sub> as a solvent. They also found that glassy alloy Pd<sub>81</sub>Si<sub>19</sub> exhibited a more than 50 times higher TOF than a conventional silica-supported palladium catalyst under similar condition toward the semihydrogenation of a propargylic alcohol. Selectivity to isophytol was 100% at low conversion but declined to 77% at around 70% conversion due

to overhydrogenation.<sup>8</sup> Finally, CoSi/SiO<sub>2</sub> synthesized by metal organic chemical vapor deposition (MOCVD) of Co(SiCl<sub>3</sub>)(CO)<sub>4</sub> showed high catalytic activity and selectivity in naphthalene hydrogenation.<sup>9</sup>

Selective hydrogenation is a simple, viable, and highly atom efficient method for removing poisoning impurities,<sup>10</sup> and one of its key technologies is the catalyst. The catalysts for selective hydrogenation of phenylacetylene mainly include supported Pd, Ni, Pt, Pb, Ru, Rh, and Cu<sup>11–15</sup> and other new catalyst materials.<sup>7,16</sup> Palladium catalysts moderated by transition metals in the feed are now used to remove phenylacetylene from styrene.<sup>10,11</sup> Ni catalysts could also hydrogenate phenylacetylene in the presence of styrene but is not satisfactory due to its low activity and selectivity.<sup>12</sup> As such, more effective catalytic materials are needed for selective hydrogenation of phenylacetylene that can afford high styrene selectivity under mild conditions.

Given the results of previous available studies, silicide-modified nickel may be a promising catalyst for selective hydrogenation of phenylacetylene. The conventional preparation methods for silicides materials generally are inherited from the microelectronic industry, including solid state reaction, molten salt method, coreduction route,<sup>17</sup> chemical vapor transport,<sup>18</sup> and chemical vapor deposition,<sup>19</sup> which result in low surface area and thus likely low catalytic performance. In the present study, a novel route to prepare silicide-modified nickel catalyst is presented. First, nanostructure NiO was produced by using carbon material as a template and nickel nitrate as a precursor. Then, the as-prepared high surface area NiO was reduced by

\* To whom correspondence should be addressed. Fax: +86-411-39893991. E-mail: changhai@dlut.edu.cn. Homepage: <http://finechem.dlut.edu.cn/liangchanghai>.

<sup>†</sup> Dalian University of Technology.

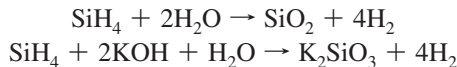
<sup>‡</sup> University of South Carolina.

$H_2$  and further silicified by 10 vol %  $SiH_4$  in  $H_2$  at relatively low temperature and atmospheric pressure. Those silicide-modified nickels showed desirable catalytic properties for selective hydrogenation of phenylacetylene. In addition, it is shown that electronic and geometrical structural properties of the silicide-modified nickel catalyst have a significant impact on both their magnetic and catalytic properties.

## 2. Experimental Section

**NiO by an Activated Carbon Route.** Ultrahigh surface area carbon material was prepared by a direct chemical activation route.<sup>20</sup> Generally, petroleum coke was reacted with excess KOH at 900 °C to produce carbon materials containing potassium salts. These salts were removed by successive water washings. The surface area of the carbon material measured by the BET method was 3234 m<sup>2</sup> g<sup>-1</sup>, the pore volume was 1.78 cm<sup>3</sup> g<sup>-1</sup>, and the average pore size was 2.2 nm. The template carbon materials were impregnated at room temperature with a saturated aqueous solution of **nickel nitrate**. The slurry was then filtered and squeezed to remove the liquid on the carbon surface.<sup>21–23,28,29</sup> After drying in air at 60 °C for 8 h, the resulting sample was transferred to a tubular furnace. The furnace was then ramped to 300 °C over 85 min in argon, and then the gas was switched to a mixture of 20%  $O_2$  in argon (120 sccm) and heated to 400 °C over 170 min. The obtained solids were designated as CT-NiO.

**Preparation of Silicide-Modified Nickel Catalyst.** Typically, the obtained CT-NiO was reduced at  $H_2$  atmosphere at 350 °C for 4 h. The long reduction time served to remove the  $H_2O$  that was produced. For the Si deposition, the water level must be low enough to prevent the formation of silicon oxides on the surface, which act as a diffusion barrier to Si.<sup>24</sup> The reduced samples were cooled to the silification temperature under the same  $H_2$  flow. Because  $SiH_4$  is explosive, experiments should be carried out cautiously. The hydrogen flow was 90 sccm while Si source ( $SiH_4$ ) was introduced into the reactor at a flow rate of 10 sccm. The resulting Ni sample reacted with a 10%  $SiH_4/H_2$  mixture at various silification temperatures for 15 min.<sup>6,25</sup> When the reaction ended,  $SiH_4$  flow was first stopped and then the product was cooled down to the room temperature (RT) in  $H_2$  (30 sccm) and passivated in 1%  $O_2/Ar$  overnight.<sup>26</sup> The obtained solids were designated as  $T_r-T_s-NiSi_x$ , where  $T_r$  referred to the reduced temperature and  $T_s$  referred to the silification temperature. The exhaust gas can be absorbed by water or alkali liquor in the silification. The reactions are as follows:



**Characterization.** Thermogravimetric/derivative thermogravimetric (TG/DTG) experiments were performed in a Mettler Toledo TGA/SDTA851e thermogravimetric analyzer. The samples were placed in an atmosphere of 80% Ar and 20%  $O_2$  and heated at 5 °C/min to the final temperature of 750 °C.

Nitrogen adsorption and desorption isotherms were constructed using the multipoint method at -196 °C and were measured using a Micrometrics 2020. Prior to the measurements, all samples were degassed completely at 200 °C in a vacuum of 10<sup>-3</sup> Torr for at least 4 h. Surface areas were calculated from the linear part of the Brunauer–Emmet–Teller (BET) plot.

X-ray diffraction (XRD) analyses of the samples were carried out using a Rigaku D/Max-RB diffractometer with a Cu  $K\alpha$  monochromatized radiation source, operated at 40 KV and 100

mA. The average size of nickel silicide particles was evaluated by the Scherrer formula as

$$L = \frac{0.9\lambda_{K\alpha_1}}{B_{(2\theta)} \cos \theta_{max}}$$

where  $\lambda_{K\alpha_1}$  is 1.54178 Å, and  $B_{(2\theta)}$  is a full width at half-maximum of diffraction peak in radians. The mole fraction  $Y_i$  of  $NiSi_x$  in a  $Ni-Ni_2Si-NiSi-NiSi_2$  mixture was calculated from XRD patterns as

$$Y_i = \frac{S_i}{S_1 + S_2 + S_3 + S_4}$$

where  $S_1$ ,  $S_2$ ,  $S_3$ , and  $S_4$  are the peak areas of the most intense reflections of Ni,  $Ni_2Si$ ,  $NiSi$ , and  $NiSi_2$ , respectively.<sup>27</sup>

Surface compositions were investigated by X-ray photoelectron spectroscopy (XPS) employing an ESCALAB250 (Thermo VG, USA) spectrometer with Al  $K\alpha$  (1486.6 eV) radiation with a power of 150 W. Survey and individual high-resolution spectra were recorded with a pass energy of 50 eV. Ni 2p, Si 2p, and O 1s lines were monitored. All core-level spectra were referenced as the C1s neutral carbon peak at 284.6 eV and were deconvoluted into Gaussian component peaks.

Magnetic measurements were preformed on a JDM-13 vibrating sample magnetometer (VSM). M/H measurements were made with applied fields up to 4000 Oe at RT and the complete hysteresis loops, characteristic of ferromagnetic behavior, were recorded.

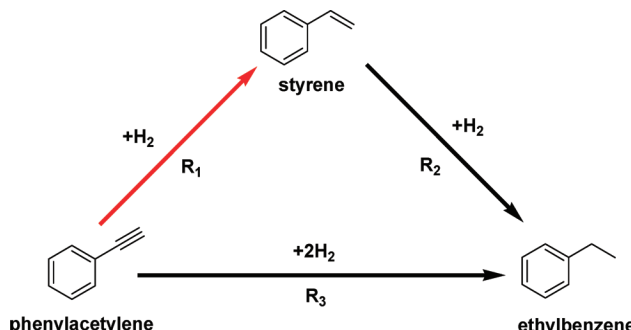
The particle size distribution of the samples was analyzed by transmission electron microscopy (TEM) (Tecnai G220 S-Twin, 200 kV). Energy dispersive X-ray spectroscopy (EDX) was also performed using the same instrument. Elemental mapping was conducted under STEM mode with the EDX detector as recorder.

Temperature-programmed reduction with  $H_2$  ( $H_2$ -TPR) was carried out using a Micromeritics AutoChem II 2920 instrument. About 100 mg of catalyst was placed in a quartz reactor, and was reduced in a stream of 10%  $H_2/Ar$  gas mixture with a flow rate of 50 sccm. The sample was heated from RT to 850 at 10 °C/min. The amount of the hydrogen consumption during the reduction was estimated by a thermal conductivity detector (TCD).

**Hydrogenation Activity Measurements.** According to the procedure previously employed,<sup>12</sup> hydrogenation runs were carried out in a closed vessel, under vigorous shaking in a conventional low-pressure hydrogenator. The catalyst was activated in an ultrapure hydrogen stream at 300 °C for 1 h, and then cooled down to RT. The vessel was filled with hydrogen to 0.27 MPa and vented three times to remove any residual air. Liquid-phase hydrogenation of phenylacetylene (Scheme 1) was carried out in a 50 mL stainless steel autoclave. The catalyst (0.2 g) was mixed with 10 mL of a 1 M ethanolic substrate solution, followed by  $H_2$  pressurization to 0.41 MPa. The reaction was carried out at 50 °C for 5 h under stirring. The products were analyzed by gas chromatography using a flame ionization detector with a SE-54/52 capillary column. A known amount of n-octane solution was used as an internal standard in the analysis.

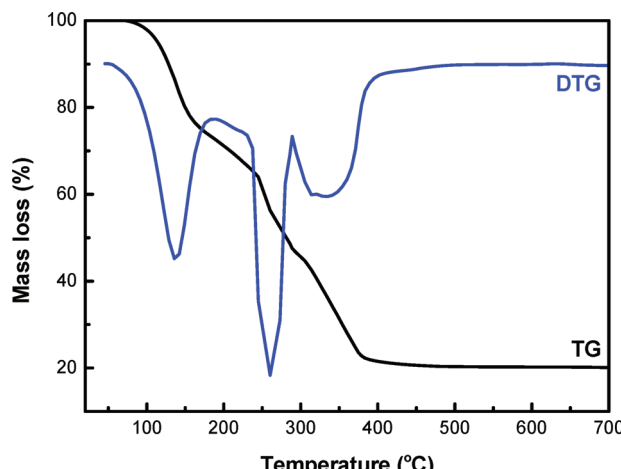
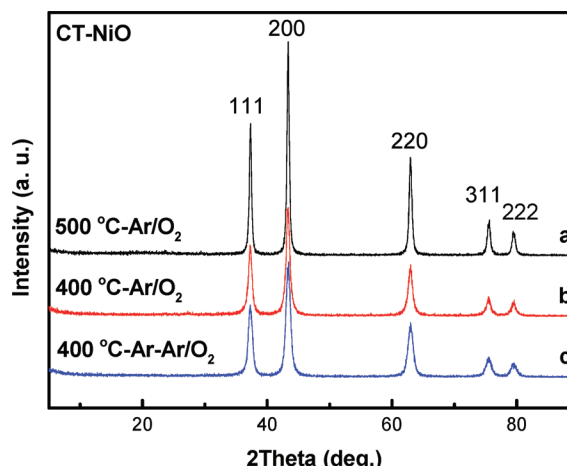
## 3. Results and Discussion

**Synthesis of NiO by an Activated Carbon Route.** Because calcination had shown an unfavorable impact on the final surface

**SCHEME 1: Reaction Pathways for the Hydrogenation of Phenylacetylene**

area of NiO, this synthetic step was studied in more detail. Figure 1 shows the TG/DTG curves of the activated carbon impregnated with a saturated aqueous solution of nickel nitrate at room temperature. As can be seen, about 24% of mass is lost from 60 to 160 °C, which is attributed to the removal of surface physisorbed water and some dehydration of the precursor. Due to the decomposition of Ni(NO<sub>3</sub>)<sub>2</sub> and the partial removal of carbon template, the maximum rate of mass loss occurs at 260 °C. The small peak at 330 °C is tentatively assigned to the further loss of carbon template and the carbon combustion is completed at temperature higher than 400 °C. As reported by Schüth et al.,<sup>28,29</sup> the presence of the metal nitrate could catalyze the combustion of the activated carbon, which in turn could induce sintering of the synthesized inorganic particles. Therefore, argon was first passed over the Ni(NO<sub>3</sub>)<sub>2</sub> impregnated activated carbon while heating to 300 °C over 85 min. The gas flow was then switched to the 20% O<sub>2</sub> in argon and the sample heated to 400 °C over 170 min to remove the carbon template completely. The obtained powders had a high surface area of about 37 m<sup>2</sup> g<sup>-1</sup>.

The XRD patterns of the as prepared NiO are displayed in Figure 2. It clearly shows the (111), (200), (220), (311), and (222) reflections of pure cubic phase NiO (JCPDS no. 47-1049). The estimated average sizes of the particles and the surface area are summarized in Table 1. It has been conclude that higher burnoff temperature would lead to sintering of the NiO particles and reduced the surface area. Furthermore, the particle size of NiO heated at 400 °C in Ar first, followed by the O<sub>2</sub>/Ar mixture (1:4) is smaller than that for only treatment in an O<sub>2</sub>/Ar mixture (1:4). Thus, it is proposed that the decomposition of nickel

**Figure 1.** TG/DTG curves of the sample Ni(NO<sub>3</sub>)<sub>2</sub> on the activated carbon.**Figure 2.** XRD patterns of the NiO prepared by carbon template route. a. Calcined at 500 °C in O<sub>2</sub>/Ar mixture (1:4). b. Calcined at 400 °C in O<sub>2</sub>/Ar mixture (1:4). c. Calcined at 400 °C in Ar first and then O<sub>2</sub>/Ar mixture (1:4).**TABLE 1: Particle Size and Surface Area of Samples Obtained by Carbon Template Route**

factor	particle size/nm	S <sub>BET</sub> (m <sup>2</sup> g <sup>-1</sup> )
500 °C-Ar/O <sub>2</sub>	20.0	7.1
400 °C-Ar/O <sub>2</sub>	15.8	16.0
400 °C-Ar-Ar/O <sub>2</sub>	12.1	37.0

nitrate first in Ar may eliminate the sintering effect caused by the nitrate and the carbon material.

**Synthesis of Silicide-Modified Nickel Catalyst by Reduction and Silification.** Figure 3 exhibits the XRD patterns of Ni and T<sub>r</sub>-T<sub>s</sub>-NiSi<sub>x</sub>. A (400 °C-CT-NiO) was reduced at 350 °C and further silicified by 10 vol % SiH<sub>4</sub> in H<sub>2</sub> at elevated temperature. B (500 °C-CT-NiO) was reduced at 450 °C and further silicified by 10 vol % SiH<sub>4</sub> in H<sub>2</sub> at elevated temperature. The crystalline phases were identified by comparing with JCPDS files (Ni, cubic, no. 04-0850; Ni<sub>2</sub>Si, orthorhombic, no. 48-1339; NiSi, orthorhombic, no. 38-0844; NiSi<sub>2</sub>, cubic, no. 43-0989). For both panels A and B in Figure 3, XRD patterns of the samples show the typical diffraction peaks at 44.51, 51.85, and 76.37°, which are due to cubic phase nickel. As shown in Figure 3A, the XRD pattern of the 350 °C-300 °C-NiSi<sub>x</sub> sample shows diffraction peaks of Ni<sub>2</sub>Si at 32.48, 39.46, 42.38, 43.49, 45.50, 48.76, 53.34, and 69.00°, indicating metal nickel is silicified to Orthorhombic phase Ni<sub>2</sub>Si. At the same time, weak peaks at 45.84 and 47.28° can be assigned to Orthorhombic phase NiSi. When the silification temperature increases to 350 °C, the diffraction peaks of NiSi become sharper while the peaks of metal nickel become weaker. By further increasing the temperature to 400 °C, four new diffraction peaks at 28.60, 47.41, 56.33, and 76.59° are observed, assigned to cubic phase NiSi<sub>2</sub>. When the temperature rises to 450 °C, the peaks of NiSi<sub>2</sub> become sharper while the peaks of NiSi become weaker. Examining the spectra more closely (insets), there is a slight peak shift, about 0.34° to higher 2θ values from 45.50° to 45.84° with the increase of silification temperature, which may be attributed to the transformation of Ni<sub>2</sub>Si (121) to NiSi (112). In addition, the XRD peak at 47.28° shifts to higher 2θ values (47.41°), corresponding to the transformation of NiSi (211) to NiSi<sub>2</sub> (220).

The phase changes as a function of silification temperature have been reported by Foggiato et al.<sup>30</sup> The first Ni<sub>2</sub>Si phase formed in the temperature range of 250–300 °C forms the basis for formation of the NiSi at higher temperature. However, too

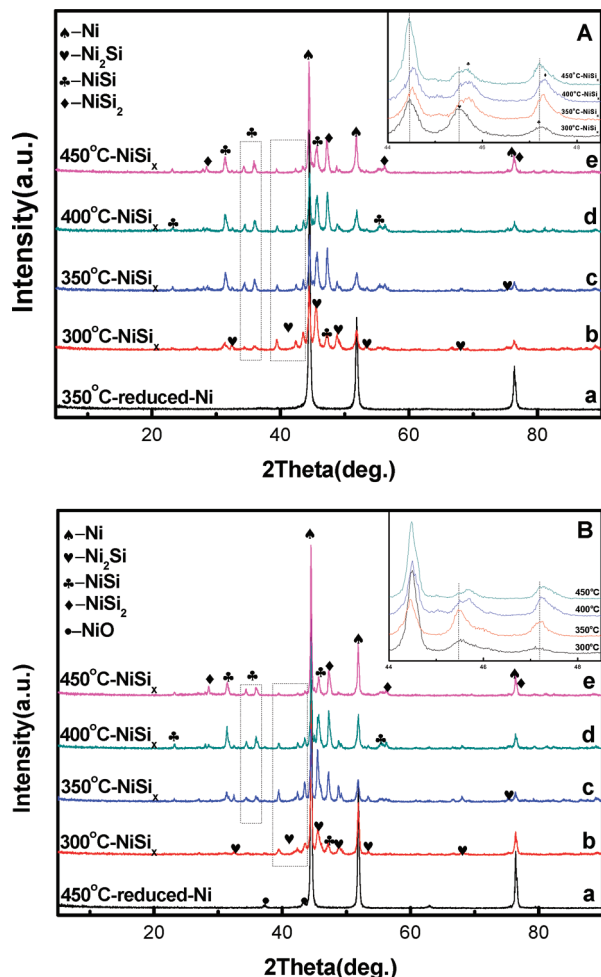


**Figure 3.** XRD patterns of Ni and silicide-modified nickel catalyst. A: 400 °C-CT-NiO were reduced at 350 °C H<sub>2</sub> and further silicidized by 10 vol % SiH<sub>4</sub> in H<sub>2</sub> at variety temperature. B: 500 °C-CT-NiO were reduced at 450 °C H<sub>2</sub> and further silicidized by 10 vol % SiH<sub>4</sub> in H<sub>2</sub> at variety temperature.

high temperature leads to the formation of NiSi<sub>2</sub>. The XRD pattern of the sample reduced at 350 °C shows the typical diffraction peaks of Ni. However, results of H<sub>2</sub>-TPR for the powders of NiO catalysts show reaction of the oxide only in 400–600 °C.<sup>31</sup> So these results suggest that the oxide reduction can be reached at atmospheric pressure and a temperature of 350 °C, as long as there is sufficient time to overcome any induction period.<sup>32</sup> The as-prepared NiO by the carbon template route may create O vacancies, which leads to an increase in the absorption energy of H<sub>2</sub> and a decrease in the energy barrier associated with the cleavage of the H–H bond.

Comparing Figure 3A with Figure 3B, it is seen that the peaks of the 350-T<sub>s</sub>-NiSi<sub>x</sub> samples are wider than that of 450-T<sub>s</sub>-NiSi<sub>x</sub>, but that the diffraction peak intensities are weaker, indicating the smaller particle sizes of 350-T<sub>s</sub>-NiSi<sub>x</sub>. In addition, Figure 3A shows that the Ni diffraction peak intensities in NiSi<sub>x</sub> reduced at 350 °C are weaker, which suggests that high surface area NiO reduced by H<sub>2</sub> is more accessible to and easier to react with SiH<sub>4</sub>. Figure 4 shows the mole fraction  $Y_i$  of NiSi<sub>x</sub> in a Ni–Ni<sub>2</sub>Si–NiSi–NiSi<sub>2</sub> mixture, calculated from XRD patterns. It is clear that the formation of nickel silicides involves the following sequence with increasing silicification temperature: Ni (cubic) → Ni<sub>2</sub>Si (orthorhombic) → NiSi (orthorhombic) → NiSi<sub>2</sub> (cubic).

Figure 5 gives the crystal structures of Ni<sub>2</sub>Si, NiSi, and NiSi<sub>2</sub>. NiSi<sub>2</sub> and Ni both have a cubic cell belonging to the Fm3m,

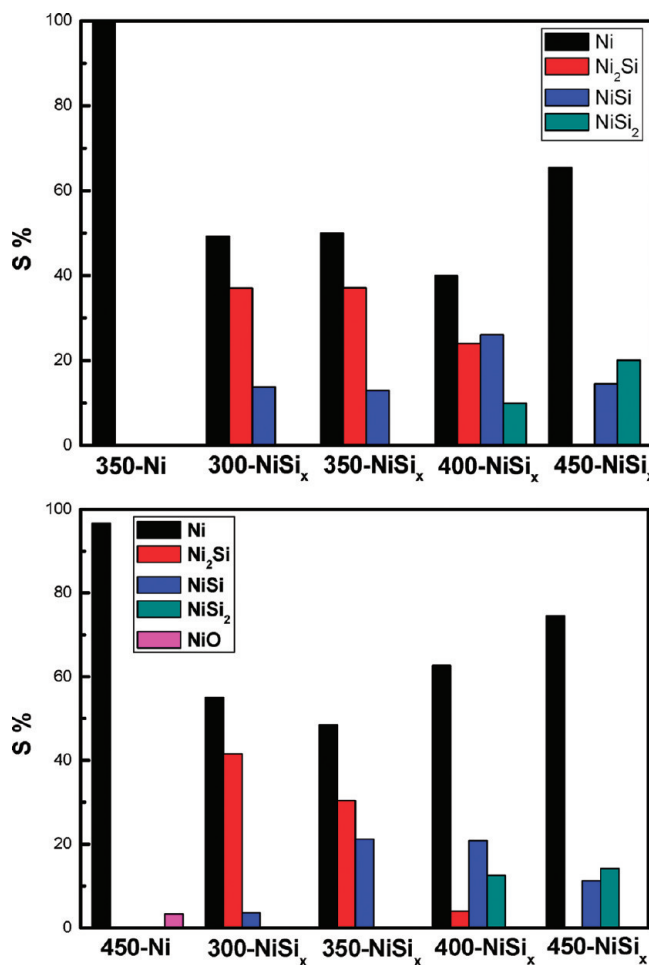


**Figure 4.** The mole fraction  $Y_i$  of NiSi<sub>x</sub> in a Ni–Ni<sub>2</sub>Si–NiSi–NiSi<sub>2</sub> mixture calculated from XRD patterns of NiSi<sub>x</sub>. A: 400 °C-CT-NiO were reduced at 350 °C H<sub>2</sub> and further silicidized by 10 vol % SiH<sub>4</sub> in H<sub>2</sub> at elevated temperature. B: 500 °C-CT-NiO were reduced at 450 °C H<sub>2</sub> and further silicidized by 10 vol % SiH<sub>4</sub> in H<sub>2</sub> at elevated temperature.

no. 225 space group, but the surface of NiSi<sub>2</sub> is characterized by alternating atoms of the two metals, so that there is no direct Ni–Ni or Si–Si bonding. The type of bonding is far different from that of pure Ni or Si;<sup>33</sup> Ni<sub>2</sub>Si has a orthorhombic cell belonging to the *Pbnm*, no. 62 space group;<sup>34</sup> NiSi has a simple orthorhombic primitive cell belonging to the *Pnma*, no. 62 (oP8 Pearson symbol) space group. The orthorhombic unit cell contains four nickel and four silicon atoms. Nickel atoms have six first silicon neighbors forming a strongly distorted octahedron, and silicon atoms have six first neighbors (nickel atoms) forming a distorted trigonal prism.<sup>35</sup>

XPS experiments were carried out to ascertain the chemical nature and type of elements present on the surface of the passivated 350–350-NiSi<sub>x</sub> and 350–450-NiSi<sub>x</sub> catalysts. Typical spectra are shown in Figure 6. In the XPS elemental survey spectra of the studied samples (Figure 6a), the presence of nickel, silicon, oxygen, and carbon could be confirmed. The atomic compositions are summarized in Table 2. Comparing the two samples, the Si/Ni ratio increases with increasing silicification temperature, which indicates that the nickel-rich silicide transforms to silicon-rich silicide by dissolving silicon atoms into the metal lattices. Since this analysis has a penetration depth less than 4 nm, the signal is expected to be from the coating layer entirely. Unfortunately, upon exposure of the silicide-modified nickel catalysts to air, the surface consists primarily of silicon oxide.<sup>36,37</sup>

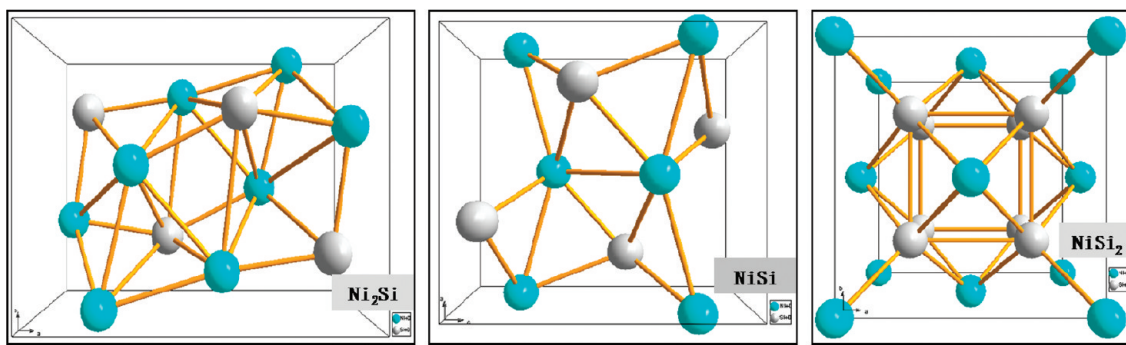
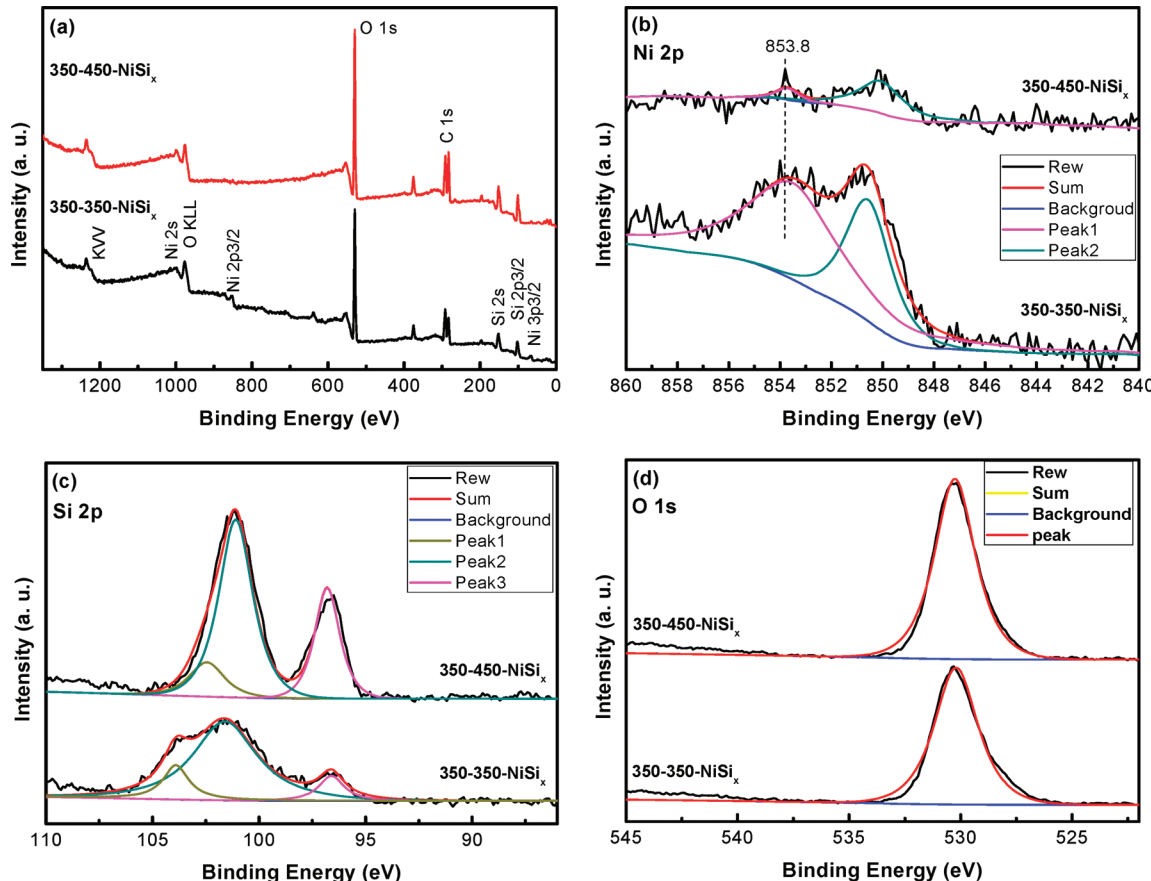
Figure 5. Crystal structures of  $\text{Ni}_2\text{Si}$ ,  $\text{NiSi}$ , and  $\text{NiSi}_2$ .

Figure 6. XPS spectra of the silicide-modified nickel nanostructures (a) survey scan; multiplex spectra of (b) Ni 2p, (c) Si 2p, and (d) O 1s.

**TABLE 2: Elemental Concentration of the Surface Coating of the Silicide-modified Nickel Nanostructures, as Determined Using Quantitative XPS**

samples	surface composition (%)		
	Si 2p	Ni 2p	O 1s
350-350-NiSi <sub>x</sub>	33.3	2.7	64.0
350-450-NiSi <sub>x</sub>	39.7	0.7	59.6

Figure 6b depicts the high-resolution Ni 2p<sub>3/2</sub> spectrum obtained from the two samples. The main band of Ni 2p<sub>3/2</sub> at 853.8 eV corresponding to  $\text{NiSi}$  is observed for all samples, which is higher than the Ni 2p<sub>3/2</sub> peak of elemental Ni (852.7 eV)<sup>38</sup> indicating the binding energy of this peak shifts to a higher position and become less intense with increasing Si content. The high-resolution Si 2p, O 1s spectra of the two samples are shown in Figures 6c and 6d, respectively. Unfortunately, due to the high concentration of silicon oxide on the surface, there is an extra broad peak at 101–104 eV in the Si

2p spectrum corresponding to  $\text{Si}-\text{O}_x$ . Moreover, the O 1s signal can be fitted with a broad peak position at 530.2 eV, which could originate from a  $\text{Ni}-\text{Si}-\text{O}$  compound formation.<sup>39</sup>

The formation of a metal silicide can be further confirmed by magnetic measurements.<sup>40</sup> Figure 7 shows the magnetization curves of the as prepared nickel nanoparticles, the  $350-T_s-\text{NiSi}_x$  samples, and the  $450-T_s-\text{NiSi}_x$  samples. All of the  $\text{NiSi}_x$  samples show a certain coercivity ( $H_c$ ) at room temperature, which is characteristic for ferromagnetic behavior in nanoparticles. The variety of the coercivity is attributed to the modification by silicon atoms and the formation of the  $\text{NiSi}_x$  phases. Their saturation magnetization values at 4000 Oe drastically decrease as Si is added to Ni. With increasing the silicification temperatures (i.e., as  $\text{Ni} \rightarrow \text{Ni}_2\text{Si} \rightarrow \text{NiSi} \rightarrow \text{NiSi}_2$ ), the saturation magnetization values first decrease, before eventually increasing. This phenomenon may be ascribed to the electronic structure of  $\text{Ni}_2\text{Si}$  and the crystal structure of  $\text{NiSi}_2$ . Jarrige et al. reported that the d states in  $\text{Ni}_2\text{Si}$  had a stronger Ni metal-like character.<sup>41</sup>

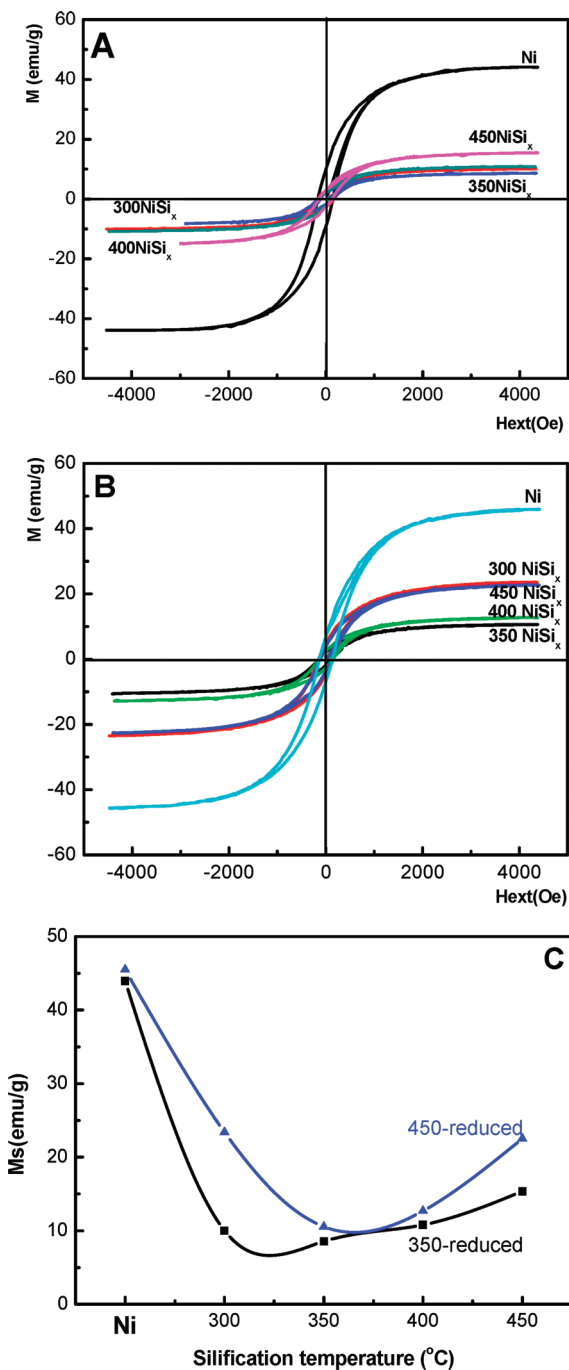


**Figure 7.** Hysteresis M/H loops at room temperatures corresponding to Ni and NiSi<sub>x</sub>. A: Produced at 350 °C H<sub>2</sub> reduced and further silicidized by 10 vol. % SiH<sub>4</sub> in H<sub>2</sub> at variety temperature. B: Produced at 450 °C H<sub>2</sub> reduced and further silicidized by 10 vol % SiH<sub>4</sub> in H<sub>2</sub> at variety temperature. C: The saturation magnetization values vs the silification temperature for silicide-modified nickel at different reduced temperature.

The magnetism of NiSi was found to be nonferromagnetic from first-principles study<sup>35</sup> and experimental findings.<sup>42</sup> From the crystal structures of Ni and NiSi<sub>2</sub> (Figure 5), it can be seen that both NiSi<sub>2</sub> and the metal nickel are cubic *Fm3m* (225) crystal structure. In addition, Figure 7C clearly shows that the saturation magnetization values of silicide-modified nickel reduced at 350 °C are smaller than those reduced at 450 °C at the same silification temperatures, which can be attributed to size effects.<sup>43,44</sup> In general,  $M_s$  values gradually increase with an increase in the grain size.

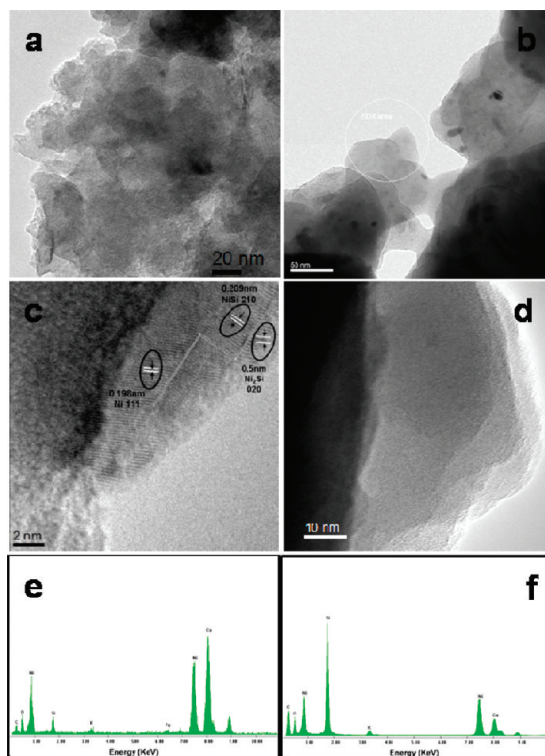


**Figure 8.** Representative low-magnification TEM image, HRTEM image, and the EDX spectrum of the NiSi<sub>x</sub> sample: (a, c, and e) 450–350-NiSi<sub>x</sub>, (b, d, and f) 450–450-NiSi<sub>x</sub>. The EDX spectra reveal that the NiSi<sub>x</sub> sample is composed of Ni, Si, and O. The Cu signals arise from the copper TEM grid and the peak of carbon is caused by contamination from irradiation of the electron beam.

From a practical standpoint, the superior magnetism exhibited by the silicide-modified nickel catalysts allows them to be easily separated from a liquid reaction mixture using a relatively low magnetic field (i.e., a small magnet). Indeed, catalysts were recovered quantitatively by simple filtration, regenerated by washing with ethanol, and dispersed for further use.

In order to investigate the structural properties and the composition distribution, TEM, HRTEM, and EDX were carried out. The representative low magnification TEM image of the 450–350-NiSi<sub>x</sub> and 450–450-NiSi<sub>x</sub> samples are shown in panels a and b of Figure 8, respectively. It can be seen that the NiSi<sub>x</sub> nanocrystals exhibit a certain sheet structure, but are aggregated to same degree. The HRTEM image of the 450–350-NiSi<sub>x</sub> sample shown in Figure 8c demonstrates that the nickel surface is overlaid with a thin layer of NiSi<sub>x</sub>, i.e., the lattice spacing of 0.25 nm corresponds to that of (020) planes of Ni<sub>2</sub>Si<sup>45</sup> and the lattice spacing of 0.21 nm corresponds to that of (210) planes of NiSi.<sup>46</sup> The EDX spectra shown in Figures 8e,f further confirm the existence of Si and Ni elements in the samples. With elevated silification temperature, the Si/Ni ratio dramatically increases, consistent with the XPS results. While samples handled in air are likely to show O contamination, homogeneous Ni, Si and O distributions were found in the passivated 450–350-NiSi<sub>x</sub> sample, as seen in the STEM dark field image and corresponding elemental maps shown in Figure 9.

The H<sub>2</sub>-TPR profiles for nickel oxide and passivated silicide-modified nickel catalysts are shown in Figure 10. For the NiO sample, NiO reduction to metallic nickel occurs with a peak temperature at around 315 °C.<sup>47</sup> For the passivated silicide-modified nickel samples, the reduction peak of NiO shifts from 315 to 258 °C with increasing silification temperature. This suggests that the nickel silicide promotes the reduction of NiO.

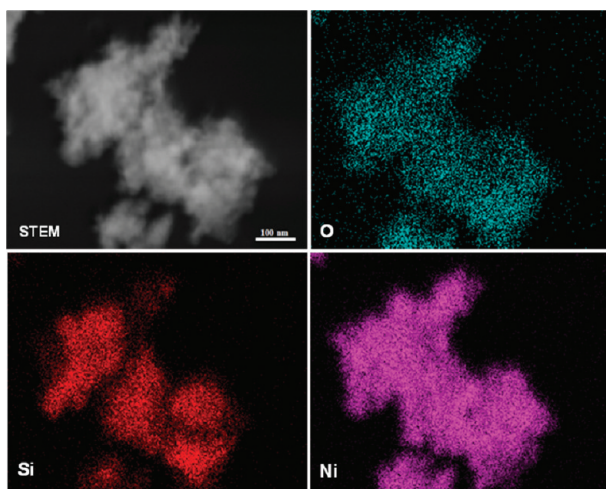


**Figure 9.** Representative STEM dark-field images and corresponding X-ray maps of O, Ni, and Si for 450–350-NiSi<sub>x</sub>.

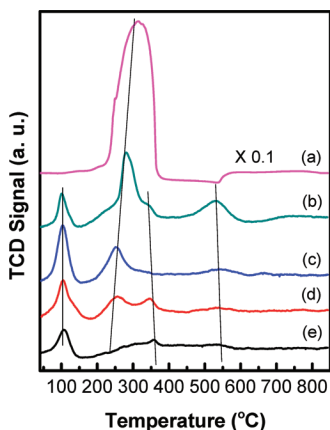


**Figure 10.** H<sub>2</sub>-TPR profiles of (a) nickel oxide and the silicide-modified nickel catalysts (b) 350–300-NiSi<sub>x</sub>, (c) 350–350-NiSi<sub>x</sub>, (d) 350–400-NiSi<sub>x</sub>, and (e) 350–450-NiSi<sub>x</sub>.

A low temperature peak at 100 °C is attributed to the silicon oxide (SiO<sub>x</sub>) coated on the surface, which is consistent with the results of XPS analysis. This oxygen does not desorb as molecular oxygen, but can be removed from the sample by a reduction in hydrogen. For the passivated silicide-modified nickel samples, one low temperature peak is observed between 340 and 360 °C. This feature is tentatively assigned to the reaction of oxygen species adsorbed on nickel silicide with H<sub>2</sub>. These results are similar to those of the TPR of CoSi/SBA-15.<sup>48</sup> In addition, the peak shifts to the higher temperature with increased silification temperature, probably due to the strong interaction of Ni with Si atoms. This result is similar to that obtained during TPR of Ni–Sn intermetallic compound particles.<sup>49</sup> The high temperature peak at 530 °C is attributed to the liberation of Si due to NiSi<sub>x</sub> decomposition in hydrogen, and the results show some similarity to those obtained for TPR of nitrides.<sup>50,51</sup> The peak shifts to the higher temperature with increased the silification temperature, probably due to the phase transition of nickel silicide. Therefore, the TPR conditions match those used for actual catalyst activation prior to hydrogenation.

**Hydrogenation Reactions.** The hydrogenation activities of the as-prepared Ni and silicide-modified nickel catalysts were tested in the liquid-phase selective hydrogenation of phenylacetylene. For each catalyst, the liquid-phase selective hydrogenation of phenylacetylene reactions was carried out using 10 mL of 1 M ethanolic phenylacetylene solution with 0.2 g catalyst in 0.41 MPa H<sub>2</sub> at 50 °C for 5 h. Figure 11 shows the

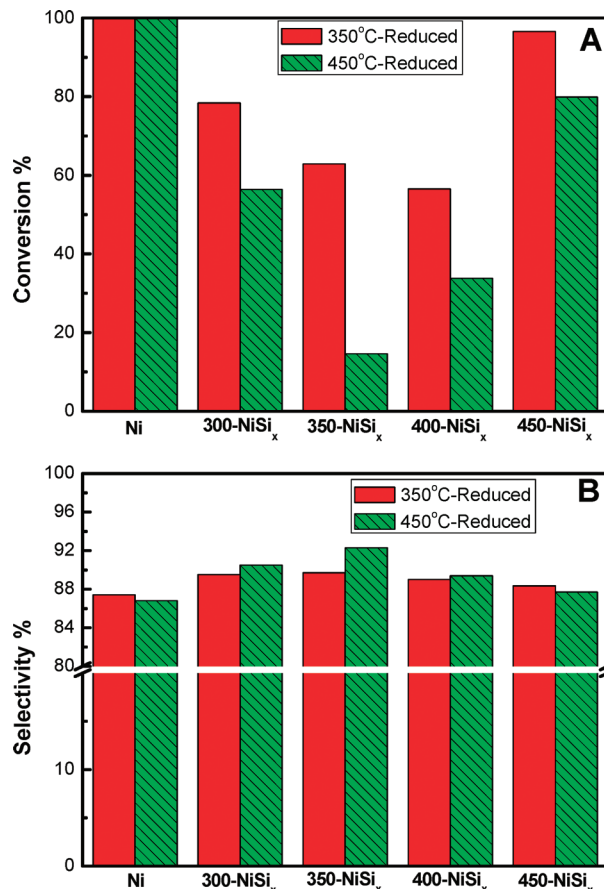


**Figure 11.** Results of liquid-phase hydrogenation of phenylacetylene over the as-prepared NiSi<sub>x</sub> catalysts (all of the reactions were performed using 10 mL of 1 M ethanolic phenylacetylene solution with 0.2 g of catalyst in 0.41 MPa H<sub>2</sub> at 50 °C for 5 h).

conversions (A) and selectivities (B) of the 450-T<sub>s</sub>-NiSi<sub>x</sub> and 350-T<sub>s</sub>-NiSi<sub>x</sub> samples in the selective hydrogenation of phenylacetylene. The latter has a higher conversion than the former, which is attributed to the poorer crystallinity after reduction at 350 °C versus 450 °C. For the series if samples reduced at 350 °C and (in the case of NiSi<sub>x</sub>) silicified at 300, 350, 400, and 450 °C, the conversions of phenylacetylene are 100, 78, 63, 57, and 97%, respectively, and the selectivity to styrene are 87, 90, 90, 89, and 88%, respectively. The conversions for the silicide-modified nickel catalyst are lower than Ni alone, while the selectivity is essentially unchanged.

As silicification temperature is increased, the conversion of phenylacetylene first decreases, followed by a dramatic increase at the highest temperature. This trend can perhaps be explained by the varying phases present in these catalysts. A previous study showed that the Ni<sub>2</sub>Si (3d<sup>8.7</sup>4sp<sup>1.2</sup>) phase has a relatively strong Ni (3d<sup>9</sup>4s<sup>1</sup>) metal-like character.<sup>52</sup> As such, it is expected to have some similar chemical and catalytic properties to metal Ni. In contrast, the NiSi phase (3d<sup>8.6</sup>4sp<sup>1.3</sup>) has electronic and crystal structures that are all significantly different from Ni, causing the fall off in catalytic activity (see Figure 11a, 350-NiSi<sub>x</sub>). Finally, when the silicification temperature reaches 450 °C, the catalyst particles had high degree of crystallinity (as shown in the XRD patterns) are partly agglomerated, which reduces the number of surface active sites to same extent. However, the NiSi<sub>2</sub> (3d<sup>8.7</sup>4sp<sup>1.5</sup>) phase prominent after this treatment has the similar crystal structure to metal Ni (cubic Fm3m 225). This may yield some similar chemical properties to Ni metal due to geometrical effects, causing the conversion

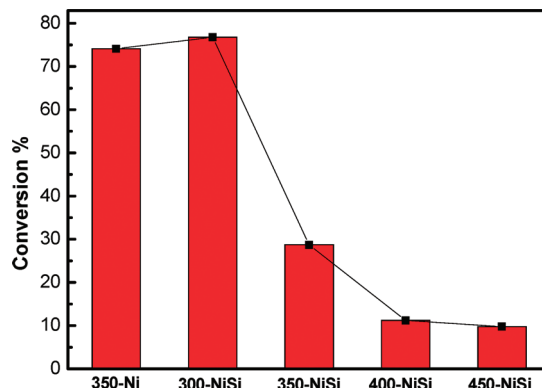


**Figure 12.** Results of liquid-phase hydrogenation of styrene over the as-prepared  $350-T_s\text{-NiSi}_x$  catalysts (all of the reactions were performed using 10 mL of 1 M ethanolic styrene solution with 0.2 g of catalyst in 0.41 MPa H<sub>2</sub> at 50 °C for 50 min).

**TABLE 3: Recycling Experiment of the Phenylacetylene Hydrogenation on the 350–350-NiSi<sub>x</sub> Catalyst**

cycle <sup>a</sup>	conversion of phenylacetylene (%)	selectivity to styrene (%)
first	66.4	88.4
second	59.9	93.0
third	25.4	94.9
after activated <sup>b</sup>	47.0	91.9

<sup>a</sup> All of the reactions were performed using 10 mL of 1 M ethanolic phenylacetylene solution with 0.2 g of catalyst in 0.41 MPa H<sub>2</sub> at 50 °C for 5 h. <sup>b</sup> The catalyst recycling 3rd used in reaction after activated by H<sub>2</sub> at 300 °C again.

of phenylacetylene to increase. Compared with the previous reports,<sup>53</sup> the as-prepared silicide-modified nickel catalysts using SiH<sub>4</sub>/H<sub>2</sub> silicification show higher activity and selectivity.

To further clarify the nature of the selective hydrogenation of phenylacetylene on silicide-modified nickel, the hydrogenation of styrene was also explored. As shown in Figure 12, for the series of samples reduced at 350 °C and (in the case of NiSi<sub>x</sub>) silicified at 300, 350, 400, and 450 °C, the conversions of styrene are 74, 77, 29, 11, and 10%, respectively. The silicide-modified nickel catalysts have lower intrinsic activity than the sample Ni, which further demonstrated that the formation of nickel silicides influenced the styrene adsorption and reduced the reaction rates of styrene hydrogenation. However, all the silicide-modified nickel catalysts can convert styrene into ethylbenzene completely at suitable time (>5 h) (the data are not shown in here). Besides, the conversion decreases with the silification temperature increase, which indicates the catalyst are aggregated at higher temperature (as shown in TEM patterns), leading to reduce the active site.

To investigate the stability of the silicide-modified Ni catalysts, the recycling experiments were carried out for phenylacetylene hydrogenation on the 350–350-NiSi<sub>x</sub> catalyst (Table 3). After the first reaction cycle, the solid catalyst was filtered off and washed 3 times with ethanol, and then the catalyst was repeatedly used under the same conditions. The conversion of phenylacetylene decrease from 66% of the first reaction cycle to 25% of the third cycle, while the selectivity to styrene increase slightly. This may be due to the active sites covered by the strong adsorbed species, the partial oxidation of the active surface during the filtration, and the sample loss in the recycle. It is noteworthy that the activity of the 350–350-NiSi<sub>x</sub> sample can be partly recovered after activated by hydrogen at 300 °C, which can be attributed to removing strong adsorbed

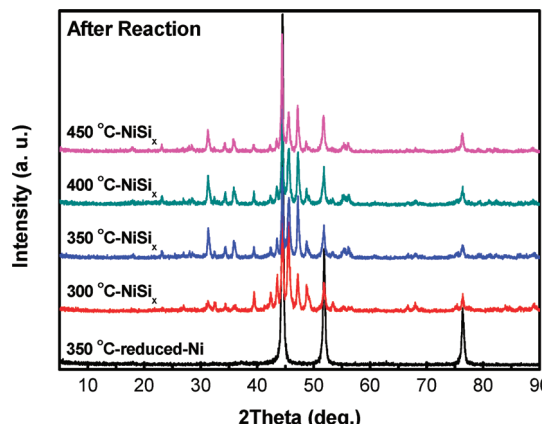


**Figure 13.** XRD patterns of Ni and silicide-modified nickel catalysts ( $350-T_s\text{-NiSi}_x$ ) after the phenylacetylene hydrogenation.

species and the oxide layer on the surface of catalyst. Besides, the structure of silicide catalysts after hydrogenation has also been investigated by XRD. Comparing Figures 3 and 13, no obvious change was observed in the XRD patterns, except that the crystallinity of Ni catalyst increased greatly. This indicated that the agglomeration of Ni particles occurred after hydrogenation of phenylacetylene in 0.41 MPa H<sub>2</sub> at 50 °C for 5 h. The structure of silicide-modified Ni catalysts have no changed obviously. It exhibited that the silicide-modified Ni is a stable and durable catalyst in the hydrogenation reaction.

#### 4. Conclusions

Nanoscale silicide-modified nickel catalysts with significant catalytic activity and high selectivity for phenylacetylene selective hydrogenation have been successfully synthesized by using the carbon template for oxides and further SiH<sub>4</sub>/H<sub>2</sub> silicification to silicides. The XRD, magnetic measurements, HRTEM, and EDX confirm the formation of NiSi<sub>x</sub> involved the following sequence, Ni (cubic) → Ni<sub>2</sub>Si (orthorhombic) → NiSi (orthorhombic) → NiSi<sub>2</sub> (cubic), with the increasing silicified temperatures. They show that Si atoms reside into the interstitial sites between Ni atoms and change the nickel unit cell lattice, make further effect the catalytic activity and selectivity. The XPS results reveal that silicon oxide primarily formed on the surface of NiSi<sub>x</sub> during exposure to air. The work also indicates that the carbon template for oxides and further SiH<sub>4</sub>/H<sub>2</sub> silicification to silicides are of great potential in controlled synthesis of transition metal silicides, which could make it possible to scale up this novel method for an industrial application with low cost and high performance in catalytic activity and selectivity.

**Acknowledgment.** We gratefully acknowledge the financial support provided by the National Natural Science Foundation of China (No. 20973029), the Program for New Century Excellent Talents in Universities of China (No. NCET-07-0133), and the Doctoral Fund of Ministry of Education of China (No. 20070141048).

#### References and Notes

- (1) Lavoie, C.; d'Heurle, F. M.; Detavernier, C.; Cabral, C., Jr. *Microelectron. Eng.* **2003**, *70*, 144.
- (2) Bhaskaran, M.; Sriram, S.; Sim, L. W. *J. Micromech. Microeng.* **2008**, *18*, 1.
- (3) Lin, Y.; Zhou, S.; Liu, X.; Sheehan, S.; Wang, D. *J. Am. Chem. Soc.* **2009**, *131*, 2772.
- (4) Zhou, F.; Szczecz, J.; Pettes, M. T.; Moore, A. L.; Jin, S.; Shi, L. *Nano Lett.* **2007**, *7*, 1649.

- (5) Thomas, H.; Maugh, I. I. *Science* **1984**, 225, 403.
- (6) Nuzzo, R. G.; Dubois, L. H.; Bowles, N. E.; Trecoske, M. A. *J. Catal.* **1984**, 85, 267.
- (7) Tschan, R.; Wandeler, R.; Schneider, M. S.; Schubert, M. M.; Baiker, A. *J. Catal.* **2001**, 204, 219.
- (8) Tschan, R.; Wandeler, R.; Schneider, M. S.; Burgener, M.; Schubert, M. M.; Baiker, A. *Appl. Catal., A* **2002**, 223, 173.
- (9) Liang, C.; Zhao, A.; Zhang, X.; Ma, Z.; Prins, R. *Chem. Commun.* **2009**, 2047.
- (10) Domínguez-Domínguez, S.; Berenguer-Murcia, Á.; Linares-Solano, Á.; Cazorla-Amorós, D. *J. Catal.* **2008**, 257, 87.
- (11) Domínguez-Domínguez, S.; Berenguer-Murcia, Á.; Pradhan, B. K.; Linares-Solano, Á.; Cazorla-Amorós, D. *J. Phys. Chem. C* **2008**, 112, 3827.
- (12) Bautista, F. M.; Campelo, J. M.; Garcia, A.; Luna, D.; Marinas, J. M.; Quiros, R. A.; Romero, A. A. *Catal. Lett.* **1998**, 52, 205.
- (13) Wilhite, B. A.; McCready, M. J.; Varma, A. *Ind. Eng. Chem. Res.* **2002**, 41, 3345.
- (14) Adams, R. D.; Captain, B.; Zhu, L. *J. Organomet. Chem.* **2006**, 691, 3122.
- (15) Pellegatta, L.; Blandy, C.; Collière, V.; Choukroun, R.; Chaudret, B.; Cheng, P.; Philippot, K. *J. Mol. Cata. A: Chem.* **2002**, 178, 55.
- (16) Punji, B.; Mague, J. T.; Balakrishna, M. S. *J. Organomet. Chem.* **2006**, 691, 4265.
- (17) Lu, Q.; Hu, J.; Tang, K.; Qian, Y.; Zhou, G.; Liu, X. *Solid State Ionics* **1999**, 124, 317.
- (18) Song, J. Y.; Schmitt, A. L.; Jin, S. *Nano Lett.* **2007**, 7, 965.
- (19) Schmitt, A. L.; Zhu, L.; Schmeißer, D.; Himpel, F. J.; Jin, S. *J. Phys. Chem. B* **2006**, 110, 18142.
- (20) Grunewald, G. C.; Drago, R. S. *J. Am. Chem. Soc.* **1991**, 113, 1636.
- (21) Liang, C.; Qiu, J.; Li, Z.; Li, C. *Nanotechnology* **2004**, 15, 843.
- (22) Liang, C.; Ma, Z.; Lin, H.; Ding, L.; Qiu, J.; Frandsen, W.; Su, D. *J. Mater. Chem.* **2009**, 19, 1417.
- (23) Liang, C.; Ma, Z.; Ding, L.; Qiu, J. *Catal. Lett.* **2009**, 130, 167.
- (24) Cabrera, A. L.; Kirner, J. F.; Pierantozzi, R. *J. Mater. Res.* **1990**, 5, 74.
- (25) Dubois, L. H.; Heights, B.; Nuzzo, R. G. U.S. Patent, 4,507,401, 1985.
- (26) Lee, K. S.; Mo, Y. H.; Nahm, K. S.; Shim, H. W.; Suh, E. K.; Kim, J. R.; Kim, J. *J. Chem. Phys. Lett.* **2004**, 384, 215.
- (27) Liang, C.; Tian, F.; Li, Z.; Feng, Z.; Wei, Z.; Li, C. *Chem. Mater.* **2003**, 15, 4846.
- (28) Schüth, F. *Angew. Chem., Int. Ed.* **2003**, 42, 3604.
- (29) Schwickardi, M.; Johann, T.; Schmidt, W.; Schüth, F. *Chem. Mater.* **2002**, 14, 3913.
- (30) Foggiato, J.; Yoo, W. S.; Ouaknine, M.; Murakami, T.; Fukada, T. *Mater. Sci. Eng., B* **2004**, 114–115, 56.
- (31) Brito, J. L.; Laine, J.; Pratt, K. C. *J. Mater. Sci.* **1989**, 24, 425.
- (32) Rodriguez, J. A.; Hanson, J. C.; Frenkel, A. I.; Kim, J. Y.; Pérez, M. *J. Am. Chem. Soc.* **2002**, 124, 346.
- (33) Nuzzo, R. G.; Dubois, L. H. *Appl. Surf. Sci.* **1984**, 19, 407.
- (34) Bisi, O.; Calandra, C. *J. Phys. C: Solid State Phys.* **1981**, 14, 5479.
- (35) Connétable, D.; Thomas, O. *Phys. Rev. B: Condens. Matter* **2009**, 79, 094101.
- (36) Dubois, L. H.; Nuzzo, R. G. *J. Vac. Sci. Technol. A* **1984**, 2, 441.
- (37) Szczecz, J. R.; Jin, S. *J. Mater. Chem.* **2010**, 20, 1375.
- (38) Tam, P. L.; Nyborg, L. *Surf. Coat. Technol.* **2009**, 203, 2886.
- (39) Saha, S. K.; Howell, R. S.; Hatalis, M. K. *Thin Solid Films* **1999**, 347, 278.
- (40) Praliaud, H.; Martin, G. A. *J. Catal.* **1981**, 72, 394.
- (41) Jarrige, I.; Capron, N.; Jonnard, P. *Phys. Rev. B: Condens. Matter* **2009**, 79, 035117.
- (42) Meyer, B.; Gottlieb, U.; Laborde, O.; Yang, H.; Lasjaunia, J. C.; Sulpice, A.; Madar, R. *J. Alloys Compd.* **1997**, 235, 262.
- (43) Hui, C.; Shen, C.; Yang, T.; Bao, L.; Tian, J.; Ding, H.; Li, C.; Gao, H.-J. *J. Phys. Chem. C* **2008**, 112, 11336.
- (44) Yamauchi, Y.; Komatsu, M.; Fuziware, M.; Nemoto, Y.; Sato, K.; Yokoshima, T.; Sukegawa, H.; Inomata, K.; Kuroda, K. *Angew. Chem., Int. Ed.* **2009**, 48, 1.
- (45) Yan, X. Q.; Yuan, H. J.; Wang, J. X.; Liu, D. F.; Zhou, Z. P.; Gao, Y.; Song, L.; Liu, L. F.; Zhou, W. Y.; Wang, G.; Xie, S. S. *Appl. Phys. A: Mater. Sci. Process.* **2004**, 79, 1853.
- (46) Kim, C. J.; Kang, K.; Woo, Y. S.; Ryu, K. G.; Moon, H.; Kim, J. M.; Zang, D. S.; Jo, M. H. *Adv. Mater.* **2007**, 19, 3637.
- (47) Znak, L.; Zieliński, J. *Appl. Catal., A* **2008**, 334, 268.
- (48) Zhao, A.; Zhang, X.; Chen, X.; Guan, J.; Liang, C. *J. Phys. Chem. C* **2010**, 114, 3962.
- (49) Onda, A.; Komatsu, T.; Yashima, T. *J. Catal.* **2001**, 210, 13.
- (50) Wei, Z.; Xin, Q.; Grange, P.; Delmon, B. *J. Catal.* **1997**, 168, 176.
- (51) Leary, K. J.; Michaels, J. N.; Stacy, A. M. *J. Catal.* **1987**, 107, 393.
- (52) Franciosi, A.; Weaver, J. H. *Phys. Rev. B: Condens. Matter* **1982**, 26, 546.
- (53) Xiao, J.; Yang, W.; Chen, Y.; Chen, X. *Ind. Catal.* **2004**, 12, 7.

JP1050832